


Optimized weak measurement of orbital angular momentum-induced beam shifts in optical reflection

WENJIN LONG,¹ JINTAO PAN,¹ XINYI GUO,² XIAOHE LIU,² HAOLIN LIN,² HUADAN ZHENG,¹ JIANHUI YU,^{1,4} HEYUAN GUAN,¹ HUIHUI LU,¹ YONGCHUN ZHONG,² SHENHE FU,² LI ZHANG,³ WENGUO ZHU,^{1,2,*}  AND ZHE CHEN¹

¹Guangdong Provincial Key Laboratory of Optical Fiber Sensing and Communications, Jinan University, Guangzhou 510632, China

²Department of Optoelectronic Engineering, Jinan University, Guangzhou 510632, China

³School of Physics and Optoelectronic Engineering, Foshan University, Foshan 528000, China

⁴e-mail: kensomyu@gmail.com

*Corresponding author: zhuwg88@163.com

Received 10 May 2019; revised 3 July 2019; accepted 11 September 2019; posted 13 September 2019 (Doc. ID 367234); published 30 October 2019

Tiny but universal beam shifts occur when a polarized light beam is reflected upon a planar interface. Although the beam shifts of Gaussian beams have been measured by the weak measurement technique, the weak measurement for orbital angular momentum (OAM)-induced spatial shifts of vortex beams is still missing. Here, by elaborately choosing the preselection and postselection states, the tiny OAM-induced Goos-Hänchen and Imbert-Fedorov shifts are amplified at an air-prism interface. The maximum shifts along directions both parallel and perpendicular to the incident plane are theoretically predicted and experimentally verified with optimal preselection and postselection states. These maximum shifts can be used to determine the OAM of vortex beams. © 2019 Chinese Laser Press

<https://doi.org/10.1364/PRJ.7.001273>

1. INTRODUCTION

Reflection and refraction at an interface between two different media are described by Snell's law and the Fresnel formula [1–5]. For a bounded beam, however, Goos-Hänchen (GH) and Imbert-Fedorov (IF) shifts occur [6]. If the incident beam carries orbital angular momentum (OAM), the OAM affects the GH and IF shifts [6]. Additional OAM-dependent terms appear in both the GH and IF shifts [6–8]. The OAM-dependent beam shifts have attracted significant attention owing to the physical interest and their applications in the determination of OAM and manipulation of optical spin [6–10]. The giant optical spin splitting induced by OAM has been predicted recently when a higher-order Laguerre-Gaussian (LG) beam transmitted through an epsilon-near-zero metamaterial slab [10]. As was demonstrated recently, the GH and IF shifts of LG beams can be optimized by carefully designing the Fresnel reflection/refraction coefficients [11]. By modulating the Fresnel coefficients via graphene, the OAM-dependent GH and IF shifts can be well tuned [12,13].

Although methods have been proposed to enhance the GH and IF shifts, they are generally small, typically a few tenths of

a wavelength [6]. A combination of a position-sensitive detector and a lock-in amplifier has to be employed to extract these tiny shifts [14]. In 2008, Hosten and Kwiat observed the spin Hall effect of light via weak measurement [15]. The spin-dependent shifts of the refracted beam from an air-prism interface were amplified and directly observed by a CCD camera [15]. The measurements of GH and IF shifts via this simple method were demonstrated by different groups through appropriately choosing the preselection and postselection states [16–20]. With the assistance of the weak measurement technique, the beam shifts have been widely used in precision metrology such as identifying the layer number of graphene and measuring thickness of Au film [21–23]. However, the weak-value amplifications for GH and IF shifts are limited within Gaussian beams. The weak measurement for OAM-induced GH and IF shifts of a vortex beam is still missing.

Here, weak-value amplification of the tiny OAM-induced shifts at an air-prism interface is demonstrated by carefully choosing the preselection and postselection states. The amplified beam shifts vary linearly with the incident OAM.

2. THEORY AND MODEL

A. Weak-Value Amplification Principle for OAM-Induced Shifts

The GH and IF shifts of vortex beams have been demonstrated by Merano *et al.* [8]. According to their work, for a vortex beam reflected from an air–prism interface, the GH shifts for horizontal (H) polarization (electric field parallel to the plane-of-incidence) and vertical (V) polarization (electric field perpendicular to the plane-of-incidence) are $X_{p,s} = 0$, while the IF shifts are $Y_{p,s} = \ell \text{Im}(\chi_{p,s})/k_0$, respectively. ℓ is the OAM of incident beam, $k_0 = 2\pi/\lambda$, with λ being wavelength in vacuum. Parameters $\chi_{p,s} = -i\partial \ln r_{p,s}/\partial\theta$, with θ being the incident angle; further, r_p and r_s are the Fresnel reflection coefficients of p and s waves at the air–prism interface, and $\chi_{p,s}$ associates with conventional GH shift for an H/V polarized Gaussian incident beam. The conventional IF shift is $\gamma_{p,s}$, where $\gamma_p = i(1 + r_s/r_p) \cot \theta$, $\gamma_s = -i(1 + r_p/r_s) \cot \theta$ [6]. One can conclude that the reflected vortex beam only undergoes IF shifts for H/V incident polarization. It is worth pointing out that these OAM-induced shifts are smaller than a wavelength.

In order to amplify the small OAM-induced shifts, the weak value technique is employed. Here, both the GH (along the x axis) and IF (along the y axis) shifts are considered. Their quantum operators can be given by [18]

$$\mathbf{GH} = \begin{bmatrix} 0 & \chi_p \\ \chi_s & 0 \end{bmatrix}, \quad (1)$$

$$\mathbf{IF} = \begin{bmatrix} \gamma_p & 0 \\ 0 & \gamma_s \end{bmatrix}, \quad (2)$$

respectively. The preselected polarization state of the system is prepared by reflecting the incident state on the prism [17]. As shown by Fig. 1(a), the incident polarization is $|\psi_{\text{in}}\rangle = \alpha|H\rangle + \beta|V\rangle$, where $\alpha = \cos \phi_1$, $\beta = \sin \phi_1$, with ϕ_1 being linear polarization angle. Thus, the preselected state is $|\psi_{\text{pre}}\rangle = \alpha r_p|H\rangle + \beta r_s|V\rangle$. The Laguerre–Gaussian (LG) mode with OAM is employed as the point state of measuring device. It is initially prepared in state $|\varphi_i\rangle = \int dx dy \varphi_i(x, y)|x, y\rangle$ [24]. The amplitude distribution of LG point is $\varphi_i(x, y) = N[x + i \text{sgn}(\ell)]^{|\ell|} \exp[-(x^2 + y^2)/w_0^2]$, where N is a normalizing constant, and w_0 is the waist of Gaussian function. The total initial state is then $|\psi_{\text{pre}}\rangle \otimes |\varphi_i\rangle$, whose evolution is dictated by the von Neumann Hamiltonian in two dimensions:

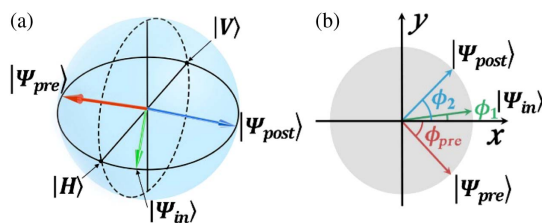


Fig. 1. (a) Incident (green arrow), preselection (red arrow), and postselection (blue arrow) states of weak-value amplification represented in Poincaré sphere. (b) Corresponding polarization angles.

$\hat{H} = g(\mathbf{GH} \otimes \hat{P}_x + \mathbf{IF} \otimes \hat{P}_y)$ [24,25]. A coupling constant g is sufficiently small, and \hat{P}_x and \hat{P}_y are the momentum observables of the probe conjugate to two commuting position observables, \hat{X} and \hat{Y} , respectively.

After the weak interaction, we postselect the system in state $|\psi_{\text{post}}\rangle = 2^{-1/2}[\exp(i\phi_2)|H\rangle + i \exp(-i\phi_2)|V\rangle]$ by combining a quarter-wave plate (QWP) and a Glan linear polarizer (GLP2). The QWP makes a fixed angle of 45° to the horizontal axis, while the GLP2 makes an angle of ϕ_2 . The point state then evolves into [24,25]

$$|\varphi_f\rangle = \langle\psi_{\text{post}}|\exp[-ig(\mathbf{GH} \otimes \hat{P}_x + \mathbf{IF} \otimes \hat{P}_y)]|\psi_{\text{pre}}\rangle|\varphi_i\rangle. \quad (3)$$

According to Refs. [25,26], the spatial displacements of the point state in the x – y plane can be calculated as

$$X_w = \langle\varphi_f|\hat{X}|\varphi_f\rangle = g[\text{Re}(A_w^{\text{GH}}) + \ell \text{Im}(A_w^{\text{IF}})], \quad (4)$$

$$Y_w = \langle\varphi_f|\hat{Y}|\varphi_f\rangle = g[\text{Re}(A_w^{\text{IF}}) - \ell \text{Im}(A_w^{\text{GH}})], \quad (5)$$

where the weak values of GH and IF operators are $A_w^{\text{GH}} = \langle\psi_{\text{post}}|\mathbf{GH}|\psi_{\text{pre}}\rangle/\langle\psi_{\text{post}}|\psi_{\text{pre}}\rangle$, $A_w^{\text{IF}} = \langle\psi_{\text{post}}|\mathbf{IF}|\psi_{\text{pre}}\rangle/\langle\psi_{\text{post}}|\psi_{\text{pre}}\rangle$, respectively. X_w and Y_w are the amplified GH and IF shifts, which both contain OAM-dependent and OAM-independent parts. These spatial shifts include not only the real part of the weak values but also the imaginary part except for $\ell = 0$ because the LG point state is not factorable in the x and y dimensions.

In the weak-value amplification, the preselection and postselection states should be nearly orthogonal. We first prepare the preselection state in diagonal state $|\psi_{\text{pre}}\rangle = 2^{-1/2}(|H\rangle - |V\rangle)$. The required incident polarization state is $|\psi_{\text{in}}\rangle = r_s/(r_p^2 + r_s^2)^{1/2}|H\rangle - r_p/(r_p^2 + r_s^2)^{1/2}|V\rangle$, with the linear polarization angle being $\phi_1 = \phi_0 = \arctan(-r_s/r_p)$. This angle is denoted as ϕ_0 in the following. When $\phi_2 = 45^\circ$, the postselection state is $|\psi_{\text{post}}\rangle = 2^{-1/2}(|H\rangle + |V\rangle)$, exactly orthogonal to the preselection state. By rotating the GLP2 a small angle from the orthogonal position, both the GH and IF shifts can be amplified (see Fig. 2). However, the amplified shifts mix the OAM-dependent and OAM-independent shifts

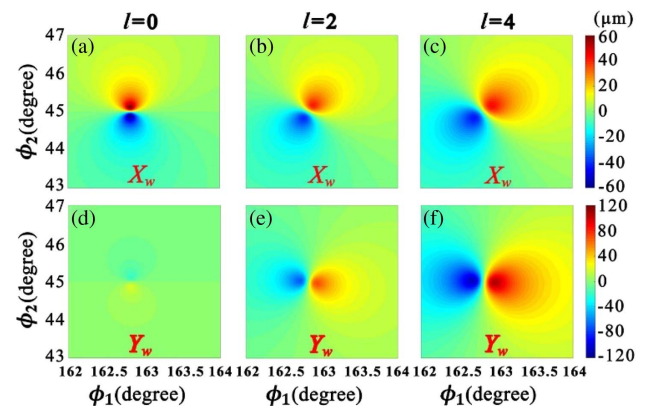


Fig. 2. GH and IF shifts of the reflected vortex beam as functions of polarization angles ϕ_1 and ϕ_2 . In the numerical calculation, $\theta = 45^\circ$, $w_0 = 125 \mu\text{m}$.

for $\ell \neq 0$. Another scheme is proposed, where we keep the postselection state $|\psi_{\text{post}}\rangle = 2^{-1/2}(|H\rangle + |V\rangle)$, and rotate the GLP1 a small angle Δ from ϕ_0 , namely, $\phi_1 = \phi_0 + \Delta$. The preselection state is then $|\psi_{\text{pre}}\rangle = [(r_p r_s + \Delta r_p^2)|H\rangle + (-r_p r_s + \Delta r_s^2)|V\rangle]/(r_p^2 + r_s^2)^{1/2}$. The polarization angle of preselection state is $\phi_{\text{pre}} \approx -\pi/4 + \Delta(r_p^2 + r_s^2)/2r_p r_s$, as shown by Fig. 1(b). From Eqs. (4) and (5), the weak-value amplified GH and IF shifts are

$$X_w = \frac{\ell r_p^2 \text{Im}(\gamma_p) - r_s^2 \text{Im}(\gamma_s)}{k_0 \Delta(r_p^2 + r_s^2)}, \quad (6)$$

$$Y_w = \frac{\ell r_s r_p [\text{Im}(\chi_p) - \text{Im}(\chi_s)]}{k_0 \Delta(r_p^2 + r_s^2)}, \quad (7)$$

where $r'_{p,s}$ is the first derivative of $r_{p,s}$, with respect to the incident angle θ . In the calculation, the coupling constant g is set to be $1/k_0$. From Eqs. (6) and (7), one finds that, with a small angle Δ , the OAM-induced GH and IF shifts can be amplified simultaneously, while the OAM-independent shifts vanish. Therefore, by elaboratively designing the preselection and postselection states, we amplified exclusively the OAM-induced shifts. Although the preselection state changes during measurement, for each small angle Δ , the postselection state is nearly orthogonal to the preselection state. The deviation of the postselection state from the orthogonal position varies with Δ ; thus, the OAM-induced shifts can be tuned by Δ .

B. Amplified OAM-Induced Shifts

We have used a quantum mechanical description to analyze the weak-value amplification principle for the OAM-induced shifts in order to provide good physical insight. However, the above theory will be invalid when Δ approaches zero. Therefore, in order to obtain a more precise analysis for the OAM-induced GH and IF shifts, we next describe them by using standard wave optics.

The incident light field after GLP1 is $\tilde{\mathbf{E}} = \tilde{\varphi}(k_x, k_y)|\psi_i\rangle$, where $\tilde{\varphi}(k_x, k_y)$ is the Fourier transformation of the LG modes $\varphi(x, y)$. k_x and k_y are the x and y components of the wave vector, respectively. The incident light field is then reflected by an air–prism interface. According to Ref. [6], the angular spectra of reflected and incident fields are connected by a 2×2 matrix. In the first-order approximation, the reflected light field can be given by [2,6]

$$\tilde{\mathbf{E}} = \left\{ \left[\alpha \left(r_p - \frac{k_x}{k_0} r'_p \right) + \beta M \frac{k_y}{k_0} \right] |H\rangle + \left[\beta \left(r_s - \frac{k_x}{k_0} r'_s \right) + \alpha M \frac{k_y}{k_0} \right] |V\rangle \right\} \tilde{\varphi}, \quad (8)$$

where $M = (r_p + r_s) \cot \theta$. The reflected light field passes through a QWP with an angle of 45° to the horizontal axis and then is selected by GLP2. The light field becomes

$$\tilde{\mathbf{E}} \propto \left\{ \left[\alpha \left(r_p - \frac{k_x}{k_0} r'_p \right) + \beta M \frac{k_y}{k_0} \right] - i \left[\beta \left(r_s - \frac{k_x}{k_0} r'_s \right) + \alpha M \frac{k_y}{k_0} \right] e^{i2\phi} \right\} \tilde{\varphi} \times (\cos \phi_2 |H\rangle + \sin \phi_2 |V\rangle). \quad (9)$$

Now the amplified shift (the beam centroid) can be straightforwardly calculated by $[X_w, Y_w] = \iint [x, y] |\tilde{\mathbf{E}}_f|^2 dx dy / \iint |\tilde{\mathbf{E}}_f|^2 dx dy$ as

$$X_w = \{ \alpha \beta r_p r_s [\text{Im}(\gamma_p e^{-i2\phi_2}) - \text{Im}(\gamma_s e^{i2\phi_2})] + \ell \alpha \beta [r_p^2 \text{Im}(\gamma_p) + r_s^2 \text{Im}(\gamma_s)] + \ell r_p r_s [\alpha^2 \text{Re}(\gamma_p e^{i2\phi_2}) - \beta^2 \text{Re}(\gamma_s e^{-i2\phi_2})] \} / k_0 W, \quad (10)$$

$$Y_w = \{ r_p r_s [\alpha^2 \text{Im}(\gamma_s e^{i2\phi_2}) - \beta^2 \text{Im}(\gamma_p e^{-i2\phi_2})] + \ell [\alpha^2 r_p^2 \text{Im}(\chi_p) + \beta^2 r_s^2 \text{Im}(\chi_s)] + \ell \alpha \beta r_p r_s [-\text{Re}(\chi_s e^{i2\phi_2}) + \text{Re}(\chi_p e^{-i2\phi_2})] \} / k_0 W, \quad (11)$$

respectively, where the energy of the light field after GLP2 is

$$W = \alpha^2 r_p^2 + \beta^2 r_s^2 + 2\alpha\beta r_p r_s \sin 2\phi_2 + (|\ell| + 1)[(\alpha r_p \chi_p)^2 + (\beta r_s \chi_s)^2] + 2\alpha r_p \beta r_s \text{Im}(\chi_p^* \chi_s e^{2i\phi_2}) + r_p^2 r_s^2 (\alpha^2 + \beta^2 - 2\alpha\beta \sin 2\phi) / k_0^2 w_0^2. \quad (12)$$

The weak-value amplified GH and IF shifts each contain three terms: one OAM-independent term and two OAM-dependent terms. Equations (10) and (11) will reduce, respectively, into Eqs. (6) and (7) when $\phi_1 = \phi_0 + \Delta$ and $\phi_2 = 45^\circ$. By tuning the angles of ϕ_1 and ϕ_2 simultaneously, the amplified GH and IF shifts can be maximized.

Figure 2 shows the amplified GH and IF shifts X_w and Y_w as functions of the polarization angles of ϕ_1 and ϕ_2 for the OAM $\ell = 0, 2, 4$, respectively. One can find from Fig. 2 that both the GH X_w and IF Y_w shifts can be amplified near point $(\phi_1, \phi_2) = (162.7^\circ, 45^\circ)$. When $\phi_1 = 162.7^\circ$, the preselection state is in the diagonal state. Both the X_w and Y_w have a positive peak and a negative peak for incident beams, with and without OAM. Without OAM ($\ell = 0$), the peak value for X_w is up to $59.4 \mu\text{m}$, while Y_w is only $19.1 \mu\text{m}$. The shifts X_w and Y_w change signs when ϕ_2 crosses 45° , where both the X_w and Y_w vanish.

For the incident beams carrying OAM ($\ell \neq 0$), the maximum values of X_w and Y_w increase with $|\ell|$. The maximum values of $|Y_w|$ are much larger than those of $|X_w|$.

Generally, both the OAM-dependent and OAM-independent terms contribute to the total shifts of vortex beams. Figure 3 compares these contributions when $\phi_2 = 44^\circ$ and $\ell = 4$. When ϕ_1 varies, the OAM-induced GH and IF shifts change signs, while the OAM-independent shifts keep. As shown in Fig. 3(b), the OAM-independent IF shift is much smaller than the OAM-dependent IF shift.

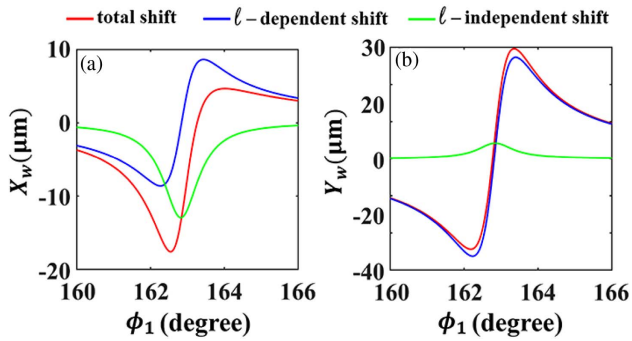


Fig. 3. Comparisons of the contributions of the OAM-dependent and OAM-independent terms in (a) GH and (b) IF shifts when $\ell = 4$, $\phi_2 = 44^\circ$.

However, when $\phi_2 = 45^\circ$, the OAM-independent terms will not contribute to the total beam shifts [see Eqs. (10) and (11)]; thus, the GH and IF shifts vanish along the line of $\phi_2 = 45^\circ$ for the case of $\ell = 0$, as shown in Figs. 2(a) and 2(d). Therefore, $\phi_2 = 45^\circ$ should be set for the amplification of OAM-induced GH and IF shifts, as discussed in Section 2.A.

C. Optimized Amplification of OAM-Induced Shifts

When $\phi_2 = 45^\circ$, the amplified GH and IF shifts are given by Eqs. (6) and (7), from which one finds that both GH and IF shifts diverge when angle Δ approaches zero. When considering Eqs. (10) and (11), however, the shifts have maximum values [27], as shown by Fig. 2.

Figures 4(a) and 4(b) show the maximum values of the amplified OAM-induced GH X_w and IF Y_w shifts changing with the incident angle θ for $\ell = 0, \pm 1, \pm 2, \pm 3$. The maximum values of X_w and Y_w are obtained by rotating the angle of GLP1 ϕ_1 for each incident angle.

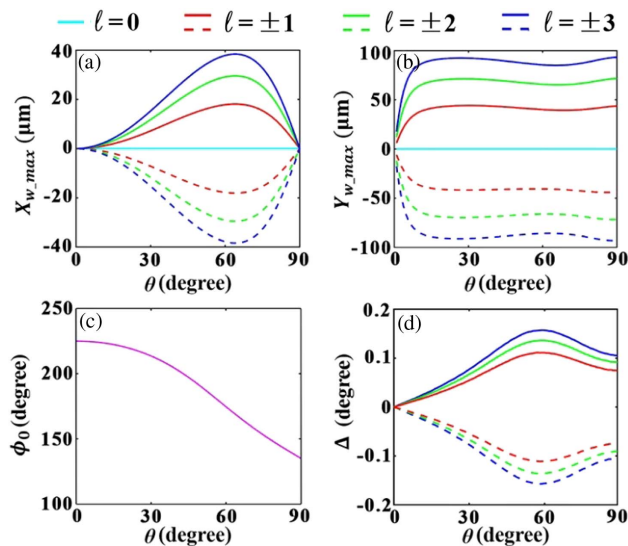


Fig. 4. Maximum OAM-induced (a) GH and (b) IF shifts changing with the incident angle. (c) Polarization angle ϕ_0 and (d) optimized angle Δ changing with the incident angle.

The maximum X_w and Y_w vary with the incident angle and increase with the OAM $|\ell|$. The maximum Y_w is almost identical for $\theta > 15^\circ$, indicating that the large OAM-induced IF shift can always be obtained by optimizing the preselection state ϕ_1 for an arbitrary incident angle of $\theta > 15^\circ$.

The optimal preselection states ϕ_1 for the OAM-induced beam shifts are found numerically for incident angle ranging from 0° to 90° . The ϕ_1 for GH X_w and IF Y_w shifts are identical. Figure 4(c) shows the angle ϕ_0 changing with the incident angle; further, ϕ_0 varies as the Fresnel reflection coefficients change with θ . The optimal deviation angle Δ ($\Delta = \phi_1 - \phi_0$) is shown by Fig. 4(d), and Δ increases with OAM $|\ell|$.

3. EXPERIMENTAL SETUP

The experiment setup is shown in Fig. 5. A Gaussian beam from a He-Ne laser is illuminated onto a vortex phase plate (VPP-m633, RPC Photonics, Inc.). The vortex phase plate containing several vortex apertures can create 1-order to 8-order vortex charges by moving its position. A circular aperture filters out scattering light. The generated vortex beam is shown in the inset in Fig. 5. The vortex beam is then focused onto a prism by a lens L1 with a focal length of 250 mm. Before the prism, a Glan polarizer GLP1 is inserted to select the incident polarization state. The reflected beam from the air-glass interface is postselected by a combination of a QWP and a polarizer GLP2. The QWP is fixed to 45° from the horizontal direction, while the GLP2 can be rotated flexibly. The combination of QWP and polarizer can flexibly design the postselection state and, thus, has been used for selective weak-value amplification of the GH and IF shifts of a Gaussian beam in partial reflection [28]. The lens L2 (focal length 25.4 mm), L3 (focal length 125 mm), and a CCD (pixel size $5.2 \mu\text{m} \times 5.2 \mu\text{m}$) form an image system with an amplification factor of 4.8 [29].

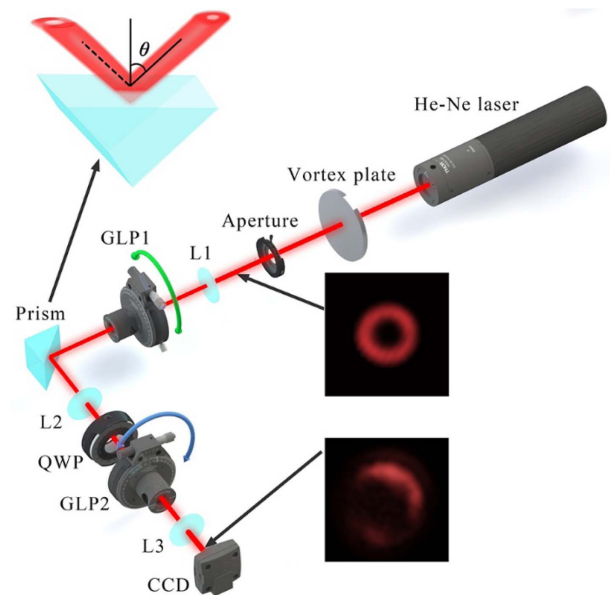


Fig. 5. Experiment setup for the measurement of OAM-induced shifts by weak technique. Insets show the intensity distributions of the generated vortex beam after aperture and the beam in the image plane of CCD with GH and IF shifts.

Therefore, the beam shifts at the air–glass interface are projected in the image plane of the CCD. All the experimental results of beam shifts below are shown in their real size and compared with the theoretical prediction.

Before measurement, we first find the incident polarization angle ϕ_0 , which results in the preselection state in diagonal state. To do this, we fix the GLP2 to be 45° and rotate the GLP1 to minimize the energy outputted from GLP2. The position corresponding to the minimum outputted energy is ϕ_0 because the preselection and postselection states are orthogonal to each other.

4. RESULTS AND DISCUSSION

By fixing $\phi_2 = 45^\circ$, the amplified GH X_w and IF Y_w shifts of vortex beams changing with ϕ_1 are measured. Figure 6 compares experimental (dots) and theoretical (lines) results when the incident angle is $\theta = 56.6^\circ$ and the OAM is $\ell = 0, 2, 4, 6$. The experimental and theoretical results do not match perfectly, although their tendencies with ϕ_1 are identical. This is because the incident beams are not in ideal shape. The vortex beams are generated experimentally by passing a Gaussian beam through a vortex phase plate. They are not perfect LG modes; the intensity fluctuates along circular rings, as shown in the inset in Fig. 5. However, the incident beam is assumed to be perfect LG modes in the theoretical calculation. The break lines in the vortex phase plate scatter light, which will enter CCD and affect the measurement of beam shifts because the vortex beams after postselected are weak.

As shown by Fig. 6, at $\phi_1 = 180^\circ$, the energy of the transmitted light field through GLP2 is weakest, namely, $\phi_0 = 180^\circ$. At this angle, there are no beam shifts with vanishing X_w and Y_w . Both the X_w and Y_w have a positive peak and a negative peak for each ℓ ($\ell \neq 0$). The positive peak positions for both X_w and Y_w are 180.20° ($\Delta = 0.20^\circ$), 180.26° ($\Delta = 0.26^\circ$), and 180.31° ($\Delta = 0.31^\circ$) for $\ell = 2, 4, 6$, respectively. The negative peak positions locate at 179.80° ($\Delta = -0.20^\circ$), 179.74° ($\Delta = -0.26^\circ$), and 179.69° ($\Delta = -0.31^\circ$), respectively. Therefore, $\Delta = \pm 0.20^\circ, \pm 0.26^\circ$, and $\pm 0.31^\circ$ are the optimal preselection states for $\ell = 2, 4$, and 6 , respectively. At optimal preselection states, the GH $|X_w|$ and IF $|Y_w|$ shifts are maximized. The maximized IF shifts are larger than GH shifts.

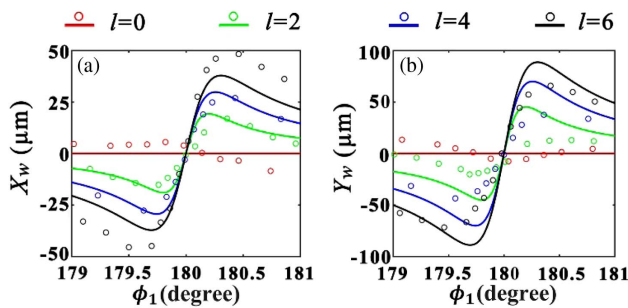


Fig. 6. Experimental (dots) and theoretical (lines) results of the amplified OAM-induced (a) GH and (b) IF shifts changing with the angle of GLP1 ϕ_1 .

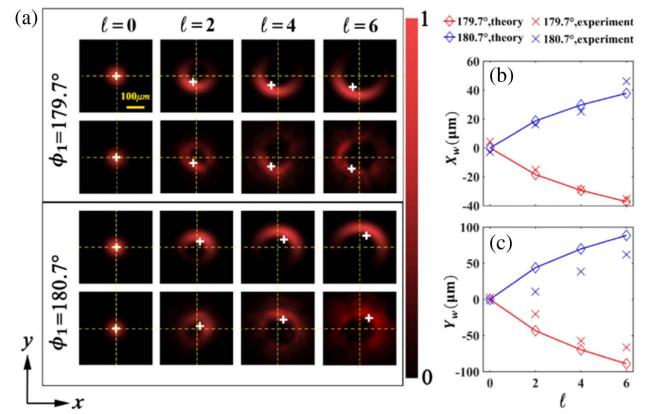


Fig. 7. (a) Comparisons of the experimental (first and third rows) and theoretical (second and fourth rows) intensity patterns of the transmitted beam from GLP2. The amplified OAM-induced (b) GH and (c) IF shifts changing with the incident OAM for $\phi_1 = 179.7^\circ$ and 180.7° .

The amplified GH and IF shifts changing with the incident OAM are investigated by fixing ϕ_1 . The intensity patterns of the transmitted beams from GLP2 for $\phi_1 = 179.7^\circ$ and 180.7° are shown in Fig. 7(a), where the theoretical and experimental results are compared for $\ell = 0, 2, 4, 6$, respectively. As shown by Fig. 7(a), the intensity patterns keep in a Gaussian beam for $\ell = 0$. For $\ell \neq 0$, and the patterns are in similar semilunar shapes, which are enlarged with the increase of ℓ . Therefore, the beam centroid moves. Figures 7(b) and 7(c) show the beam shifts along x and y axes, respectively. The theoretical and experimental GH shifts match well. The small mismatches of the theoretical and experimental IF shifts may result from the unideal vortex incident beam. Both the GH and IF shifts

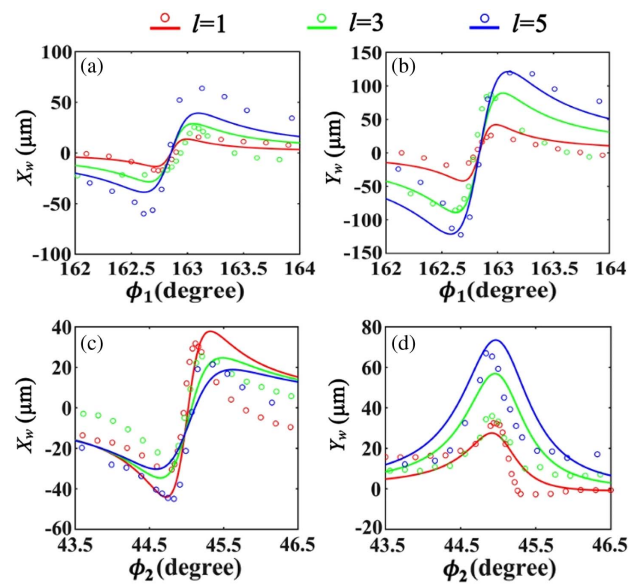


Fig. 8. Experimental (dots) and theoretical (lines) results of the amplified OAM-induced (a), (c) GH and (b), (d) IF shifts changing with (a), (b) ϕ_1 for $\phi_2 = 45^\circ$ and (c), (d) ϕ_2 for $\phi_1 = 163.3^\circ$.

increase gradually with ℓ . Thus, the amplified GH and IF shifts can be used to measure the OAM. The weak measurement scheme should be precisely as discussed in Ref. [30], and the required elements (polarizer, QWP, and prism) are frequently used in optical labs.

Figure 8 shows the amplified GH X_w and IF Y_w shifts of vortex beams changing with angles ϕ_1 and ϕ_2 when the incident angle $\theta = 45^\circ$ and the OAM $\ell = 1, 3, 5$, respectively. The experimental and theoretical results match each other. The amplified shifts can be tuned by both ϕ_1 and ϕ_2 . The maximum shift is up to 121.2 μm obtained experimentally at $\phi_1 = 163.3^\circ$ and $\phi_2 = 45^\circ$.

5. CONCLUSIONS

In conclusion, the OAM-induced GH and IF shifts of vortex beams have been simultaneously amplified by the weak measurement technique. By properly choosing the preselection and postselection states, the OAM-induced GH and IF shifts can be maximized. Notably, the IF shifts can always be maximized for an arbitrary angle larger than 15° . The IF shift is up to 121.2 μm for $\ell = 5$, $\phi_1 = 163.3^\circ$, and $\phi_2 = 45^\circ$. The maximum shifts increase with the incident OAM gradually. We believe the proposed weak measurement scheme for a vortex beam has potential applications in identifying OAM and exploiting the joint weak values of single-particle operators.

Funding. National Natural Science Foundation of China (11604050, 61475066, 61675092, 61705086); Natural Science Foundation of Guangdong Province (2016A030311019, 2016A030313079, 2016TQ03X962, 2017A010102006, 2017A030313359, 2017A030313375); Science Technology Project of Guangzhou (201604040005, 201605030002, 201704030105, 201707010396, 201803020023).

REFERENCES

- X. Ling, X. Zhou, K. Huang, Y. Liu, C. W. Qiu, H. Luo, and S. Wen, "Recent advances in the spin Hall effect of light," *Rep. Prog. Phys.* **80**, 066401 (2017).
- W. Zhu, L. Zhuo, M. Jiang, H. Guan, J. Yu, H. Lu, Y. Luo, J. Zhang, and Z. Chen, "Controllable symmetric and asymmetric spin splitting of Laguerre–Gaussian beams assisted by surface plasmon resonance," *Opt. Lett.* **42**, 4869–4872 (2017).
- K. Y. Bliokh, C. T. Samlan, C. Prajapati, G. Puentes, N. K. Viswanathan, and F. Nori, "Spin-Hall effect and circular birefringence of a uniaxial crystal plate," *Optica* **3**, 1039–1047 (2016).
- H. Lin, B. Chen, S. Yang, W. Zhu, J. Yu, H. Guan, and H. Lu, "Photonic spin Hall effect of monolayer black phosphorus in the terahertz region," *Nanophotonics* **7**, 1929–1937 (2018).
- X. Zhou, S. Liu, Y. Ding, L. Min, and Z. Luo, "Precise controlling of positive and negative Goos-Hänchen shifts in graphene," *Carbon* **149**, 604–608 (2019).
- K. Y. Bliokh and A. Aiello, "Goos-Hänchen and Imbert-Fedorov beam shifts: an overview," *J. Opt.* **15**, 014001 (2013).
- K. Y. Bliokh, I. V. Shadrivov, and Y. S. Kivshar, "Goos-Hänchen and Imbert-Fedorov shifts of polarized vortex beams," *Opt. Lett.* **34**, 389–391 (2009).
- M. Merano, N. Hermosa, J. P. Woerdman, and A. Aiello, "How orbital angular momentum affects beam shifts in optical reflection," *Phys. Rev. A* **82**, 023817 (2010).
- W. Löffler, A. Aiello, and J. P. Woerdman, "Observation of orbital angular momentum sidebands due to optical reflection," *Phys. Rev. Lett.* **109**, 113602 (2012).
- M. Jiang, W. Zhu, H. Guan, J. Yu, H. Lu, J. Tan, J. Zhang, and Z. Chen, "Giant spin splitting induced by orbital angular momentum in an epsilon-near-zero metamaterial slab," *Opt. Lett.* **42**, 3259–3262 (2017).
- Z. Xiao, H. Luo, and S. Wen, "Goos-Hänchen and Imbert-Fedorov shifts of vortex beams at air left-handed-material interfaces," *Phys. Rev. A* **85**, 33–35 (2012).
- L. Zhuo, W. Long, M. Jiang, W. Zhu, H. Guan, J. Tang, J. Yu, H. Lu, J. Zhang, and Z. Chen, "Graphene-based tunable Imbert-Fedorov shifts and orbital angular momentum sidebands for reflected vortex beams in the terahertz region," *Opt. Lett.* **43**, 2823–2826 (2018).
- W. Zhu, M. Jiang, H. Guan, J. Yu, H. Lu, J. Zhang, and Z. Chen, "Tunable spin splitting of Laguerre-Gaussian beams in graphene metamaterials," *Photon. Res.* **5**, 684–688 (2017).
- X. Yin and L. Hesselink, "Goos-Hänchen shift surface plasmon resonance sensor," *Appl. Phys. Lett.* **89**, 261108 (2006).
- O. Hosten and P. Kwiat, "Observation of the spin Hall effect of light via weak measurements," *Science* **319**, 787–790 (2008).
- S. Nechayev, M. Neugebauer, M. Vorndran, G. Leuchs, and P. Banzer, "Weak measurement of elliptical dipole moments by C-point splitting," *Phys. Rev. Lett.* **121**, 243903 (2018).
- S. Chen, C. Mi, L. Cai, M. Liu, H. Luo, and S. Wen, "Observation of the Goos-Hänchen shift in graphene via weak measurements," *Appl. Phys. Lett.* **110**, 031105 (2017).
- S. Goswami, M. Pal, A. Nandi, P. K. Panigrahi, and N. Ghosh, "Simultaneous weak value amplification of angular Goos-Hänchen and Imbert-Fedorov shifts in partial reflection," *Opt. Lett.* **39**, 6229–6232 (2014).
- G. Jayaswal, G. Mistura, and M. Merano, "Weak measurement of the Goos-Hänchen shift," *Opt. Lett.* **38**, 1232–1234 (2013).
- L. Luo, X. Qiu, L. Xie, X. Liu, Z. Li, Z. Zhang, and J. Du, "Precision improvement of surface plasmon resonance sensors based on weak-value," *Opt. Express* **25**, 21107–21114 (2017).
- X. Zhou, L. Sheng, and X. Ling, "Photonic spin Hall effect enabled refractive index sensor using weak measurements," *Sci. Rep.* **8**, 1221 (2018).
- X. Zhou, Z. Xiao, H. Luo, and S. Wen, "Experimental observation of the spin Hall effect of light on a nanometal film via weak measurements," *Phys. Rev. A* **85**, 043809 (2012).
- X. Zhou, X. Ling, H. Luo, and S. Wen, "Identifying graphene layers via spin Hall effect of light," *Appl. Phys. Lett.* **101**, 251602 (2012).
- G. Puentes, N. Hermosa, and J. P. Torres, "Weak measurements with orbital-angular-momentum pointer states," *Phys. Rev. Lett.* **109**, 040401 (2012).
- H. Kobayashi, G. Puentes, and Y. Shikano, "Extracting joint weak values from two-dimensional spatial displacements," *Phys. Rev. A* **86**, 053805 (2012).
- B. de L. Bertúlio, S. Azevedo, and A. Rosas, "Simplified algebraic description of weak measurements with Hermite-Gaussian and Laguerre-Gaussian pointer states," *Opt. Commun.* **331**, 194–197 (2014).
- X. Zhou, X. Li, H. Luo, and S. Wen, "Optimal preselection and postselection in weak measurements for observing photonic spin Hall effect," *Appl. Phys. Lett.* **104**, 051130 (2014).
- S. Goswami, S. Dhara, M. Pal, A. Nandi, P. K. Panigrahi, and N. Ghosh, "Optimized weak measurements of Goos-Hänchen and Imbert-Fedorov shifts in partial reflection," *Opt. Express* **24**, 6041–6051 (2016).
- Z. Chen, L. Zhuo, W. Zhu, L. Chen, J. Yu, H. Guan, H. Lu, J. Dong, W. Qiu, and Z. Chen, "Measurement of giant spin splitting of reflected Gaussian beams," *IEEE Photon. J.* **10**, 4500307 (2018).
- J. Qiu, C. Ren, and Z. Zhang, "Precisely measuring the orbital angular momentum of beams via weak measurement," *Phys. Rev. A* **93**, 063841 (2016).